Stochastic Upscaling of Hydrodynamic Dispersion and Retardation Factor in a Physically and Chemically Heterogeneous Tropical Soil

Vanessa A. Godoy[1,2*], Lázaro Valentin Zuquette[1] and J. Jaime Gómez-Hernández[2]

[1] Geotechnical Engineering Department, São Carlos School of Engineering, University of São Paulo. Avenida Trabalhador São Carlense, 400, 16564-002, São Carlos, São Paulo, Brazil.

[2] Institute for Water and Environmental Engineering, Universitat Politècnica de València, Camí de Vera, s/n, 46022, València, Spain

[*] corresponding author: valmeida@usp.br (+55)16 35739501

Abstract

Stochastic upscaling of flow and reactive solute transport in a tropical soil is performed using real data collected in the laboratory. Upscaling of hydraulic conductivity, longitudinal hydrodynamic dispersion, and retardation factor were done using three different approaches of varying complexity. How uncertainty propagates after upscaling was also studied. The results show that upscaling must be taken into account if a good reproduction of the flow and transport behavior of a given soil is to be attained when modeled at larger than laboratory scales. The results also show that arrival time uncertainty was well reproduced after solute transport upscaling. This work represents a first demonstration of flow and reactive transport upscaling in a soil based on laboratory data. It also shows how simple upscaling methods can be incorporated into daily modeling practice using commercial flow and transport codes.

Keywords: column experiments, spatial variability, macrodispersion coefficient, hydraulic conductivity upscaling, stochastic analysis

1. Introduction

Solute transport numerical modeling is a powerful tool to predict aquifer response in a remediation plan, to evaluate the impact of a radioactive underground repository on the biosphere, to verify the efficacy of geological materials to be used as liners in landfills, to

assess health risks due contaminant exposure, or to be used in decision-making processes (Bellin et al., 2004; Dagan, 2004; Feyen et al., 2003a, 2003b). Numerical models require input parameters that must be determined reliably to guarantee the quality of their predictions (Willmann et al., 2006).

Hydraulic conductivity (K) and transport parameters such as hydrodynamic dispersion coefficient (D), dispersivity (α) and retardation factor (R) are, generally, determined in the laboratory at a scale of a few centimeters (fine scale) (Jarvis, 2007; Jellali et al., 2010; Logsdon Keller and Moorman, 2002; Osinubi and Nwaiwu, 2005; Tuli et al., 2005; Vanderborght et al., 2000). Modeling water flow and solute transport at a fine-scale resolution is impractical, especially when modeling must be repeated many times, such as in stochastic analyses (Feyen et al., 2003a; Lawrence and Rubin, 2007).

Numerical simulations are performed in a scale of meters to kilometers (coarse scale), using equivalent parameters, homogeneous in each model cell (Wen and Gómez-Hernández, 1996). This implies a simplification of the problem since not all fine-scale information is transferred to the coarse scale (Bellin et al., 2004; Fernàndez-Garcia and Gómez-Hernández, 2007). In addition, the lack of exhaustive information implies uncertainty on flow and transport predictions, which should also be taken into account when performing upscaling (Fernàndez-Garcia and Gómez-Hernández, 2007; Gómez-Hernández and Wen, 1994; Li et al., 2011a).

We face two main problems in solute transport modeling. The first one is how to treat parameter spatial heterogeneity and the second one is how to account for the difference of scales between measurements and modeling scales (Dagan, 1989; Gómez-Hernández et al., 2006; Taskinen et al., 2008). The first problem can be tackled by using geostatistical techniques such as simulation or estimation that permit a coherent assignment of values at locations where measurements were not taken based on the values observed at measurement locations (Capilla et al., 1999; Cassiraga et al., 2005; Journel and Gomez-Hernandez, 1993; Li et al., 2011b; Morakinyo and Mackay, 2006; Wen et al., 1999; Zhou et al., 2012, 2010). The second problem can be solved by defining upscaling rules that incorporate subgrid heterogeneity of the parameters that control flow and solute transport, and that transfer the information obtained at the fine scale onto the

coarse scale to be used in the numerical code (Deng et al., 2013; Fernàndez-Garcia and Gómez-Hernández, 2007; Li et al., 2011b).

The upscaling of hydraulic conductivity is well established in the literature and several approaches have been reported, showing the limitations and effectiveness of local and non-local upscaling methods for the reproduction of water flow patterns under different types of heterogeneity (Cadini et al., 2013; Cassiraga et al., 2005; Fernàndez-Garcia and Gómez-Hernández, 2007; Gómez-Hernández et al., 2006; Li et al., 2011a; Lourens and van Geer, 2016; Renard and de Marsily, 1997; Sánchez-Vila et al., 1996; Selvadurai and Selvadurai, 2014; Wen and Gómez-Hernández, 1996). However, upscaling hydraulic conductivity only is not enough to reproduce the fine-scale transport behavior at the coarse scale due to the loss of K heterogeneity present at the fine scale that influences solute transport behavior (Cassiraga et al., 2005; Journel et al., 1986; Scheibe and Yabusaki, 1998). Fernàndez-Garcia and Gómez-Hernández (2007) proposed a method to compensate for the loss of information due to hydraulic conductivity upscaling, consisting of introducing an enhanced block hydrodynamic dispersion tensor and found that the median travel times of the breakthrough curves (BTC) were well reproduced but the tails were not.

While less common than flow upscaling studies, some solute transport upscaling works can be found in the literature showing the characteristics and limitations of different transport upscaling methods using deterministic and stochastic approaches of varying complexity (Bellin et al., 2004; Cadini et al., 2013; Cassiraga et al., 2005; Fernàndez-Garcia et al., 2009; Fernàndez-Garcia and Gómez-Hernández, 2007; Gómez-Hernández et al., 2006; Moslehi et al., 2016; Salamon et al., 2007; Tyukhova and Willmann, 2016; Vishal and Leung, 2017; Xu and Meakin, 2013).

Most transport upscaling studies are based on synthetic experiments for nonreactive solute transport and focus on the upscaling of only a single transport parameter, for example, the hydrodynamic dispersion or the retardation factor. There is still a lack of studies that intend to define upscaling rules based on real data from laboratory experiments of reactive solute transport in heterogeneous soils. In addition, to the best of our knowledge, performing upscaling considering at the same time the heterogeneity of

dispersivity and retardation factor at the local scale has not been discussed in the literature. Determining equivalent transport parameters in tropical soils, present in many regions of the world and related to important engineering problems, has not been performed before; this is a gap we also aim to reduce.

The purpose of this study is to propose upscaling rules for reactive solute transport, using fine-scale data obtained at the laboratory from water flow and reactive solute transport experiments using undisturbed tropical soil columns. We must clarify that in this work we are not investigating chemical reactions but only sorption (due to physical retention and/or adsorption) (Freeze and Cherry, 1979). A solute will be considered nonreactive when the retardation factor, R, is equal to one, while it will be considered reactive when is larger than one.

Differently from earlier studies (Fernàndez-Garcia et al., 2009; Fernàndez-Garcia and Gómez-Hernández, 2007), we use a Simple Laplacian-with-skin method to upscale hydraulic conductivity (Gómez-Hernandez, 1990; Li et al., 2011b) in order to obtain the best reproduction of water flow as observed at the fine scale. In line with the work by Fernàndez-Garcia and Gómez-Hernández (2007), we use the Enhanced Macrodispersion Coefficient approach but, as a novelty, the determination of the macrodispersion coefficient was made by considering also the heterogeneity of dispersivity, α, at the local scale. To study the upscaling of retardation factor, the p-norm approach, i.e., power averaging of the cell values within the block, was used to compute an equivalent R after a prior analysis to determine an optimal exponent p (Gómez-Hernández et al., 2006a). Contrasting with the majority of previous studies that focused on a single realization, we perform a stochastic analysis to study the variability of the upscaled parameters but also the propagation of uncertainty after upscaling. The assessment of the upscaled models is based on the reproduction at the coarse scale of the breakthrough curves (BTC) obtained at the fine scale at a selected control plane.

2. Upscaled transport model

The Macrodispersion method as described by Fernàndez-Garcia and Gómez-Hernández (2007) was used to upscale the local-scale hydrodynamic dispersion, thus accounting for

the reduction of within-block heterogeneity. The retardation factor was upscaled using the p-norm approach. These two methods were used for their simplicity and for its readiness to use in commercial transport codes based on the classical advection-dispersion equation (ADE). In this section, some details about them are provided. We recognize that sometimes the use of the ADE at the coarse scale may be inadequate to reproduce reactive solute transport at the fine scale, as discussed in previous studies (Fernàndez-Garcia et al., 2009; Li et al., 2011b). Because of that, we also intend to show the possible limitations of the use of the ADE to upscale transport solute parameters.

2.1. Hydrodynamic dispersion upscaling using the ADE

At the fine scale, the flow equation, assuming steady-state flow in the absence of sinks and sources for an incompressible fluid in a saturated porous media, is given by

$$\nabla.(\mathbf{K}^f(x)\nabla h(x))=0. \quad (1)$$

This equation results of combining Darcy's Law and the continuity equation, where h is the piezometric head, $\mathbf{K}^f$ is a second-order symmetric hydraulic conductivity tensor (observed at the fine scale), x represents the spatial location, ∇ is the gradient operator, and $\nabla \cdot$ the divergence operator.

Assuming that Fick's law is appropriate at the local scale, solute transport is given by the ADE equation, which is a mass balance equation, written, for a nonreactive solute, as

$$n^f \frac{\partial C(\mathbf{x},t)}{\partial t} = -\nabla.\left(\mathbf{q}(x)C(x,t)\right)+\nabla.(n^f(\mathbf{D}^f\nabla C(x,t)), \quad (2)$$

where $\mathbf{q}$ is the Darcy velocity given by $q(\mathbf{x}) = - \mathbf{K}^f(\mathbf{x})\nabla h(\mathbf{x})$, n^f is the porosity, C is the solute concentration, and $\mathbf{D}^f$ is the local hydrodynamic dispersion coefficient tensor with eigenvalues given by

$$\mathbf{D}_i^f = D_m + \alpha_i \frac{|\mathbf{q}^f|}{n^f}, \quad (3)$$

where D_m is the effective molecular diffusion coefficient and α_i are the local dispersivity coefficients. The dispersivitiy values parallel and transverse to the flow direction are designated as longitudinal and transverse dispersivities, α_L and α_T.

Eq.(1)(1) and Eq.(2) are used to solve the water flow and transport equations at the fine scale, respectively. However, due to the need to solve those problems on a grid coarser than the scale of the measurements, it is necessary to use block equivalent parameters (hereafter, block properties will be identified by the subscript b). According to Fernàndez-Garcia and Gómez-Hernández (2007), a block equivalent hydraulic conductivity tensor, $\mathbf{K}_b$, must preserve the fine-scale average flux through the block. Whereas a block equivalent hydrodynamic dispersion tensor, $\mathbf{D}_b$, should consider not only the dispersive fluxes at the fine scale (herein referred to as fine scale hydrodynamic dispersion) but also should account for the loss of spreading caused by the homogenization of the hydraulic conductivities. The enhanced block hydrodynamic dispersion tensor $\mathbf{D}_b$ includes an equivalent fine-scale local dispersivity (α_{eq}) plus a macrodispersivity term (A_i), which is computed so as to increase the dispersion in the upscaled (homogeneous) block. Using α_{eq} and A_i to compute $\mathbf{D}_b$ is known as the Macrodispersion approach; the resulting macrodispersion tensor is

$$\mathbf{D_b}=D_m+(\alpha_{eq}+A_i)\frac{|\mathbf{q}^f|}{n^f}. \quad (4)$$

The term A_i is constant over time but varies in space among blocks. According to Gelhar et al. (1992), A_i can range from meters to kilometers while α_{eq} ranges in the order of millimeters. Based on a literature review, Zech et al. (2015) showed that macrodispersivities can range from millimeters to meters. In this paper, block equivalent dispersivities will be named $\alpha_b = \alpha_{eq} + A_i$.

In the macrodispersion approach, upscaling is based on the macrodispersion concept (Gelhar and Axness, 1983) and the resulting transport equation to be used at the coarse scale has the same form as the local ADE at the fine scale, but replacing the local hydrodynamic dispersion tensor by the new macrodispersion tensor.

2.2. Upscaling of the retardation factor

The governing equation of solute transport subject to advection, hydrodynamic dispersion, and sorption in a physically and chemically heterogeneous aquifer at the fine scale can be expressed as

$$\frac{\partial C(\mathbf{x},t)}{\partial t}+\frac{\rho_d}{n^f}\frac{\partial S(\mathbf{x},t)}{\partial t}=-\frac{1}{n^f}\nabla.\left(\mathbf{q}(\mathbf{x})C(\mathbf{x},t)\right)+\frac{1}{n^f}\nabla.(\mathbf{D}^f\nabla C(\mathbf{x},t)), \quad (5)$$

where ρ_d is the matrix bulk density and *S* is the nonaqueous-phase concentration of sorbed solutes. The relation between C and S is established through a sorption isotherm. The simplest sorption isotherm function assumes that sorption is instantaneous, reversible and that the concentration of sorbed solutes onto the solid is directly proportional to the concentration of dissolved solutes (Freeze and Cherry, 1979). The constant of proportionality between C and S is the distribution coefficient (K_d)

$$K_d(x)=\frac{S(x)}{C(x)}\geq 0, \quad (6)$$

which quantifies the interaction between the contaminants and the soil particles. This parameter is spatially variable and its variation can exert a key role in the behavior of the solute plumes (Brusseau, 1998; Brusseau and Srivastava, 1999; Robin et al., 1991). There is no consensus about the cross-correlation between K_d and K. According to Robin et al. (1991), this correlation, in real fields, may range from weakly negative to mildly positive. In the studied soil, a very weakly negative correlation between lnK and K_d was found (-0.02) and because of that, we assumed no correlation between them.

The retardation factor R is related to K_d by,

$$R(x)=1+\frac{\rho_d}{n^f(x)}K_d(x), \quad (7)$$

and can be interpreted as the ratio of the average fluid velocity (v) ($v = q(x)/n^f$) to the velocity at which the solute propagates (v_s) (Freeze and Cherry, 1979)

$$R(x)=\frac{v}{v_s}\geq 1. \quad (8)$$

When the solutes do not interact with the solid medium (i.e., they are nonreactive), R = 1. Solutes with R > 1 are called reactive solutes (Freeze and Cherry, 1979; Shackelford, 1994).

It is important to mention that in FEFLOW (the computer code used in this work) R is expressed as a function of the Henry's adsorption constant, k [-], as

$$R(x) = 1 + \frac{1-n^f}{n^f} k(x). \quad (9)$$

Including R in the transport equation by combining Eq. (5) and Eq. (7) results in the reactive transport equation given by:

$$\frac{\partial C(\mathbf{x},t)}{\partial t} R(x) n^f + \nabla . \left(n^f v(x) C(\mathbf{x},t) \right) = \nabla . \left(\mathbf{D}^f \nabla C(\mathbf{x},t) \right). \quad (10)$$

The information obtained at the fine scale cannot be used directly at the coarse scale and it is necessary to calculate a block equivalent retardation factor R_b representative of the heterogeneity of the retardation factor within the block. This block value must be able to reproduce the mass flux breakthrough curve (BTC) obtained at the fine scale simulation when applied to the transport equation with homogeneous parameters within model blocks at the coarse scale.

Since the reproduction of the complete BTC is impossible to achieve, it is necessary to select which part of the BTC one would like to reproduce best, according to the objective of the numerical modeling (Gómez-Hernández et al., 2006).

For the calculation of R_b, the p-norm (power averaging) of R(x) can be used

$$R_b = \left(\frac{1}{V} \int_V R_f^p(\mathbf{x}) d\mathbf{x} \right)^{\frac{1}{p}}, \quad (11)$$

where V indicates the volume of the block and R_f represents the retardation factors at the fine scale. Depending on the power exponent used, the p-norm will be more affected by the low values, or by the high values within the block. In this approach, the challenge is to find the exponent p that will result in an R_b that best reproduces, at the coarse scale, the transport observed at the fine scale; to find it, numerical simulations must be performed. This technique follows the line of the power averaging equation used for calculating equivalent hydraulic conductivity by (Gómez-Hernández and Gorelick, 1989; Journel et al., 1986).

3. Field characterization

3.1. Studied soil

The studied tropical soil is found on lithologies belonging to the Botucatu Formation in São Carlos City (21°51′38″ S, 47°54′14″ W), located in the East-Center of São Paulo State (Brazil). It consists of fine-grained to medium-sized sandstones, with a reddish color, well-selected grains, high sphericity, and very friable or silicified. Cenozoic sediments are the parental material of the studied soil and cover the Botucatu Formation. These sediments are constituted by unconsolidated sands with a thickness ranging from 5 m to 7 m, and can be found in the interior of São Paulo (Azevedo et al., 1981; Giacheti et al., 1993).
The study area is a parallelepiped with dimensions Δx = 12 m, Δy = 8 m, and Δz = 4 m, from where the soil samples were taken. At the laboratory, the soil was characterized as clayey sand with macropores and double porosity fabric, an important characteristic in terms of water flow and solute transport. The main minerals present in the studied soil are quartz, kaolinite, and gibbsite, what is in accordance with Giachetti *et al.* (1993) and Kronberg *et al.* (1979). We found a small average amount of organic matter (2.40%) in this soil, common in lateritic acidic soils (Mahapatra et al., 1985). Average values of 5.71 and 5.19 for pH in H_2O and KCl, were obtained, respectively, therefore, the soil can be considered strongly acidic, a typical characteristic of Cenozoic sediments and lateritic soils (Fagundes and Zuquette, 2011; Giacheti et al., 1993).

The negative ΔpH (-0.52) and a point of zero charge (PZC) (4.67) lower than the pH_{H2O} indicate a predominance of negative charges, which can promote cation adsorption (Fagundes and Zuquette, 2011). The soil has a low cation exchange capacity (CEC) (mean value of 2.51 cmolc Kg^{-1} and maximum value of 4.20 cmolc Kg^{-1}), suggesting a low capacity to adsorb cations by electrostatic adsorption (Fagundes and Zuquette, 2011).

3.2. Experimental determination of water flow and transport parameters

In order to characterize the hydraulic conductivity and the transport parameters, 55 undisturbed cylindrical soil samples of 0.10 m diameter and 0.15 m height were taken in

the domain described earlier. In the laboratory, K was measured under constant-head conditions, with a hydraulic gradient equal to one, using a rigid-wall permeameter, at a constant temperature of 20 ºC.

The total porosity was computed as $n_t = 1-\rho_d/\rho_s$, where ρ_s is the particle density, calculated as 2.71 $Mg \cdot m^{-3}$. The effective porosity, used in the transport model, is equal to the total porosity minus the porosity that corresponds to the soil water content at 33 kPa, a suction equivalent to the field capacity (Ahuja et al., 1984; Brutsaert, 1967; Corey, 1977; Dippenaar, 2014).

When steady-state flow was reached in the flow tests, miscible displacement tests were performed. A solution 2.56 mol m^{-3} KCl (made up of 100 mg L^{-1} K^+ and 90.7 mg L^{-1} Cl^-, and referred to as the initial concentration, C_0) was continuously injected into the soil column. Solute displacement tests were also carried out under constant hydraulic head and isothermal (20 °C) conditions. The concentration (C) was measured at preset time intervals and the BTC's were determined at the outlet. Since in this work we are interested in reactive transport, only the results related to the reactive solute (potassium ion, K^+) are discussed.

The advection-dispersion equation (ADE) used to interpret the BTCs is

$$R\,\frac{\partial C}{\partial t} = D\,\frac{\partial^2 C}{\partial x^2} - v\,\frac{\partial C}{\partial x}, \qquad (12)$$

where C is the solute concentration [ML^{-3}], D is the hydrodynamic dispersion coefficient [M^2T^{-1}], R is the retardation factor [-], x is the distance [L], and t is the time [T].

When the initial condition is C = 0 for the entire sample, and the boundary conditions are $C = C_0$ at the inlet and C = 0 at an infinite distance from the inlet, Eq (12) has the following analytical solution,

$$\frac{C(t)}{C_0} = \frac{1}{2}\left[\operatorname{erfc}\left(\frac{RL-vt}{2\sqrt{DRt}}\right)\right] + \frac{1}{2}\exp\left(\frac{vL}{D}\right)\operatorname{erfc}\left(\frac{RL+vt}{2\sqrt{DRt}}\right), \qquad (13)$$

where erfc(·) is the complementary error function

This expression was fitted to the observed BTCs for each soil sample and values of the hydrodynamic dispersion and the retardation factor were obtained for both K^+ and Cl^-. The fitting was performed using the computer program CFITM (van Genuchten, 1980),

that is part of the Windows-based computer software package Studio of Analytical Models (STANMOD) (Šimůnek et al., 1999). From the values of the hydrodynamic dispersion obtained after the fitting, the dispersivity values were calculated using the relation

$$D = \alpha \cdot v . \quad (14)$$

The fit of the experimental BTC to the ADE model was evaluated by its R^2. Most BTCs presented significant tailing, R^2 ranged from 0.77 to 0.99 with a mean of 0.92. We conclude that the experimental data can be properly described by the ADE model.

3.3. Spatial variability

The exploratory statistics of the 55 measurements of the studied variables (K, n, α, and R) are summarized in Table 1. K, R and α displayed high variability (Fu and Gómez-Hernández, 2009; Robin et al., 1991; Wilding and Drees, 1983), on the contrary, the porosity presented a very low variability (Wilding and Drees, 1983).

The measured K and α values are best fitted by lognormal distributions. The lognormal model implies that the natural logarithms of K (lnK) and α (lnα) are modeled by Gaussian distributions. The normality of lnK and lnα was confirmed by the Kolmogorov-Smirnov test with a 95% confidence interval. The measured porosity and retardation factor could not be fitted by a normal distribution and they were transformed into normal variables using an empirical anamorphosis (also known as a normal-score transform). All transformed variables were standardized to normal distributions of mean zero and variance one. Variogram analysis was performed in the standardized variables lnK, n, lnα, and R.

Geostatistical techniques were used to build a model of the spatial variability of the parameters with the purpose of estimating the properties at unsampled locations (Goovaerts, 1999). The theory of geostatistics is based on the random function model assumption, where variables are modeled as spatially correlated random variables. Within this framework, it is possible to perform coherent inferences about a variable and its spatial variability.

Using the Stanford Geostatistical Modeling Software (SGeMS) (Remy, 2004), we conclude that the 55 measurements showed a spatial variability that can be modeled by an isotropic spherical variogram of the form

$$\gamma(\mathbf{h})=c_0+c_1.\mathrm{sph}(|\mathbf{h}|,a), \quad (15)$$

where *a* is the range, c_0 is the nugget effect, c_1 is the sill, **h** is the directional lag distance, and sph(·) is the spherical function. We have decided to use an isotropic variogram after investigating the ranges of the variograms in several directions and observing that there is no a significant difference on the continuity patterns as orientation changes. Due to the limited number of samples in the vertical direction, we assumed that the spatial correlation obtained for the horizontal direction is the same in the vertical direction. This choice can also be justified by the absence of clear anisotropies in the soil; it is well known that the spatial correlation anisotropy is, among other reasons, the responsible for the flow anisotropy (Lake, 1988). Table 2 shows the parameters of the variogram models used to fit the isotropic experimental variograms.

The variograms of the solute transport parameters contain a nugget effect, which implies short-scale spatial variability and/or measurement error. According to the nugget-to-total-sill ratio classification, these variables had a moderate spatial dependence (Cambardella et al., 1994).

4. Numerical simulations

4.1. Simulation of the random fields

Within the random field theory (Griffiths and Fenton, 2008; Vanmarcke, 1983), the variables, lnK, lnα, n—actually its normal-score transform—, and R—actually, its normal-score transform—are modeled as random variables at each location in space. These random variables are represented by a probability density function (pdf) that measures the likelihood that the random variable takes a specific value at a given location (Cassiraga et al., 2005). First- and second-order stationary Gaussian random fields were used to model all variables. A Gaussian random field is completely defined by its first two moments, mean and variance, and its autocorrelation function, and it is represented by the infinite set of multivariate Gaussian distributions that can be built with any combination of points within some spatial domain (Griffiths and Fenton, 2008; Vanmarcke, 1983).

Thirty equally-likely and conditioned realizations of lnK, n, lnα and R were generated using the Sequential Gaussian Simulation (SGS) algorithm as implemented in the code

GCOSIM3D (Gómez-Hernández and Journel, 1993) using the variogram functions whose parameters are shown in Table 2. The lnK random field domain is a parallelepiped with dimensions of Δx = 24 m, Δy = 16 m and Δz = 8 m and it is discretized in 3 072 000 cubic cells of side 0.1 m; each cell is of the magnitude of the permeameter measurements. The lnK domain is twice the size of the studied area because the lnK upscaling technique demands a skin composed by a certain number of additional elements (Gómez-Hernandez, 1990). However, only the inner domain of size Δx = 12 m, Δy = 8 m and Δz = 4 m was used to simulate and compare flow at the coarse and fine scales. The random fields of the other variables, conditioned on the 55 measurements, were generated in a domain equal to the studied area (Δx = 12 m, Δy = 8 m and Δz = 4 m) and discretized in 384 000 cubic cell of side 0.1 m since no skin was necessary in their upscaling methods.

The number of realizations analyzed here may be considered small for performing a rigorous estimation of uncertainty. However, since our objective is to identify trends and the impact of the upscaling in uncertainty propagation, we believe that a set of 30 realizations is enough. Before performing water flow and solute transport numerical simulations, all realizations were back-transformed according to the cumulative distribution functions of the measured data. Fig. 1a-d shows the realization number 1 of all variables (in real space, that is, after back transformation) K, n, α and k (Henry coefficient related to R by Eq. (9)).

4.2. Flow and transport solutions

The finite element method (FEM) with a pre-conditioned conjugate-gradient algorithm as implemented in FEFLOW 7.1 was used to solve the water flow and solute transport for each one of the 30 realizations (Diersch, 2014). The realizations of hydraulic conductivity were used as input parameter to the flow model while the realizations of dispersivity and retardation factor were used as input parameters to the solute transport models. We recognize that the effect of a heterogeneous variable porosity can affect the solute transport behavior, but, due to its very low variability (see Table 2) and to the necessity to reduce the dimensionality of the problem, a homogeneous value of porosity, equal to the arithmetic mean of the 55 observations, was considered for all numerical models at the fine scale.

The numerical domain is a parallelepiped discretized into 120 x 80 x 40 cubic cells of 0.1 m by 0.1 m by 0.1 m for a total of 384 000 elements. The transport mapping method (also called transfinite interpolation) algorithm was used to generate the rectangular mesh.

Steady-state flow was simulated by considering a confined problem under a constant gradient set to one to reproduce the laboratory conditions. The boundary conditions were no-flow at the top and bottom faces and constant-head was set equal to 50 m at the left face and to 38 m at the right face, forcing flow from left to right. The specific discharge in the x-direction (q_x) was calculated for each realization at a control plane, positioned on the exit face, orthogonal to the flow direction.

Reactive solute transport was simulated by adopting a first-type boundary condition at the left side, using a mass concentration of 100 mg/L (Fig. 2). At the top and bottom faces, no mass flow boundary condition was assumed. The solute transport was modeled as transient for a period of 35 days for the nonreactive problems and 100 days for the reactive ones. The time discretization was made based on a grid Courant number of 0.04. The BTCs were obtained at the exit plane of the domain (right side).

4.3. Upscaling of water flow

A Simple Laplacian-with-skin method was used to upscale the hydraulic conductivity (Gómez-Hernandez, 1990; Li et al., 2011b) in order to obtain the best reproduction of water flow at the fine scale. The whole domain, heterogeneous at the fine scale, was replaced by a unique homogeneous block, i.e., the size of the equivalent block coincides with the field site extension without intermediate resolutions (both for water flow and solute transport). The effectiveness of K upscaling was evaluated by comparing the mean specific discharge in the x-direction (q_x) at the control plane computed at the fine and coarse scales, and it was quantified by the relative bias of the specific discharge (RB_q)

$$RB_q = \frac{1}{NR}\sum_{i=1}^{NR}\left[\frac{q_{f,i}-q_{c,i}}{q_{f,i}}\right]100, \qquad (16)$$

where NR is the number of realizations; $q_{f,i}$ is the specific discharge through a control plane obtained from the numerical modeling at the fine-scale for realization i, and $q_{c,i}$ is the specific discharge through the same control plane at the coarse-scale for realization i.

4.4. Upscaling of hydrodynamic dispersion

The upscaling of hydrodynamic dispersion was done by using the Macrodispersion approach. According to this, to determine the block equivalent hydrodynamic dispersion (D_b) it is necessary to calculate α_b, that is, the sum of the equivalent fine-scale local dispersivity (α_{eq}) plus the macrodispersivity term (A_i). Both A_i and α_{eq} were calculated based on the first- and second-order moments of the BTC at the exit plane (positioned on the far right of the domain), using the expression (Wen and Gómez-Hernández, 1998)

$$\alpha_{eq} \text{ or } A_i = \frac{L}{2}\frac{\sigma_t^2}{T_a^2}, \tag{17}$$

where L is the block length, T_a is the average of the arrival times, and σ_t^2 is the variance of the arrival times.

The determination of the α_{eq} and A_i was made by solving a local transport problem releasing solute mass from one side of the block and collecting it at the opposite side, then, T_a and σ_t^2 were computed from the BTC at the exit plane. We used two scenarios of nonreactive solute transport to obtain α_b. In scenario 1, first, for each realization at the fine scale, purely advective transport was solved by using a heterogeneous K, allowing us to calculate the macrodispersion coefficients associated with the heterogeneity of K (A_i). Second, K was assumed homogeneous, and transport was solved with a heterogeneous α, allowing us to calculate the equivalent dispersivities (α_{eq}). Lastly, A_i and α_{eq} were summed up to give the α_b. In short, in scenario 1, we determined separately α_{eq} and A_i and then added them up to calculate α_b. In scenario 2, the heterogeneity at the local scale of both K and α was simultaneously considered and, for each realization, a transport problem at the local scale was solved from which α_b was directly determined using Eq. (17). Table 3 summarizes the conditions adopted in each scenario. Fig. 3 shows a cross-plot between the α_b determined in both scencarios. The results show that approach in scenario 2 can be used to quantify directly the effects of the local-scale heterogeneity of both α and K, since the results obtained by the two scenarios are very similar, with a relative bias of only 4.2 %.

The performance of hydrodynamic dispersion upscaling was evaluated by comparing the BTCs at the exit plane obtained from the fine- and coarse-scale models. These comparisons were also done for a few points of the BTC, more precisely, at the mean (T_{mean}), 5% (early, $T_{05\%}$), 50% (median $T_{50\%}$) and 95% (late, $T_{95\%}$) arrival times. It is important to mention that the selection of the part of BTC used to calculate the upscaled transport parameters is a very important step for the correct application of upscaled transport parameters in daily practice. According to Fu and Gómez-Hernández (2009) and Gómez-Hernández et al. (2006), early arrival times must be well reproduced if, for example, the objective of the transport model is the design of an underground repository for toxic or radioactive waste; median arrival times, if the objective is to asses health risks associated with contaminant exposure by drinking water (Lemke et al., 2004), and late arrival times, if the objective is to design a remediation plan. Failing to take this into account will yield under- or overestimation of the arrival times critical for the purposes of the study.

For each arrival time mentioned before, the mismatch between the concentrations obtained at the fine and coarse scales was quantified by the relative bias of the hydrodynamic dispersion (RB_d), expressed as

$$RB_d = \frac{1}{NR}\sum_{i=1}^{NR}\left[\frac{c_{f,i}-c_{c,i}}{c_{f,i}}\right]100\,, \qquad (18)$$

where $c_{f,i}$ is the concentration through a control plane obtained from the numerical modeling of a nonreactive solute at the fine scale for realization i, and $c_{c,i}$ is the concentration of the same nonreactive solute through the same control plane at the coarse-scale for the same realization.

The uncertainty analysis of the nonreactive solute transport modeling was performed by comparing the ensembles of BTCs obtained at the fine and coarse scales at the exit plane. Also, the cumulative frequency distributions obtained at the fine and coarse scales for the mean, early, median and late arrival times were compared.

4.5. Upscaling of retardation factor

The upscale of retardation factor was performed by solving the reactive solute transport at the fine scale considering K, α and R as heterogeneous and uncorrelated. Solute mass was released from one side of the block and collected at the opposite side and then the BTCs at the exit plane were computed. From these BTCs, R was inversely determined by using Eq. (13). The resulting values were considered as the equivalent ones (R_{eq}), and, from them, the exponent p that yields a p-norm of the fine values that gives results as close to R_{eq} as possible is chosen. Since the purpose is to observe only the effects of chemical heterogeneity, R was subdivided into physically driven (related to hydraulic conductivity heterogeneity) and chemically driven.

When solute arrived earlier in the coarse scale transport model than in the fine scale solution, a calibration parameter named "fictitious" retardation factor (R_f) was added to each solute transport model to retard the arrival times and improve the prediction capacity of the macrodispersion method as suggested by Cassiraga et al. (2005). This retardation factor does not represent chemical heterogeneity, but rather a delay associate with the physical heterogeneity that is removed after upscaling. To calculate R_f, we measured the solute velocity at the early, mean, median and late arrival times relative to the velocity of the same problem solved with a homogeneous R = 1, and then we quantified R_f as the ratio between the "apparently" retarded solute and the non-retarded solute for each arrival time.

We determined an exponent p for each realization individually. The optimization of the value of p was obtained using the MATLAB function called "fminbnd" based on a golden-section search and parabolic interpolation (Brent, 1973; Forsythe et al., 1976) that minimizes the objective function

$$error(p)=\left|R_{eq}- R_b\right|. \quad (19)$$

Solute transport models were then solved at the coarse-scale using the R_b determined by the best p-norm. The assessment of the R upscaling was made by comparing the BTC obtained at the coarse scale to the ones obtained at the fine scale. These comparisons

were made for the entire BTC, and for the mean, early, median and late arrival times. It was quantified by the relative bias of retardation factor (RB_R), given by

$$RB_R = \frac{1}{NR}\sum_{i=1}^{NR}\left[\frac{c_{fr,i}-c_{cr,i}}{c_{fr,i}}\right]100, \qquad (20)$$

where $c_{fr,i}$ is the reactive solute concentration through a control plane obtained from the numerical modeling at the fine scale for realization i, and $c_{cr,i}$ is the reactive solute concentration through the same control plane at the coarse scale for the same realization. The uncertainty analysis of the reactive solute transport modeling was performed in the same way as that of the nonreactive solute transport.

5. Results and discussion

5.1. Hydrodynamic dispersion upscaling

The relative bias of the specific discharge during hydraulic conductivity upscaling was only 0.8% indicating that the upscaling method worked well at the coarse scale in reproducing the water flow obtained at the fine scale. Fig. 4 shows the BTCs of realization number 30 at the fine scale and after upscaling for three situations: 1) upscaling only K, 2) upscaling using macrodispersion approach, and 3) upscaling using macrodispersion approach with a calibration term named fictitious retardation factor that will be discussed further on.

As demonstrated by others in the literature (Cassiraga et al., 2005; Journel et al., 1986; Scheibe and Yabusaki, 1998), upscaling only K, even using an advanced non-local method, is not enough to reproduce the BTCs at the coarse scale. When only the K upscaling is done, the coarse scale BTC overestimates the early arrival times and underestimate the late arrival ones. Since the K upscaling worked very well, the overestimation of the equivalent K could not explain such behavior. This finding was also reported by Li et al. (2011b) and Fernàndez-Garcia and Gómez-Hernández (2007). Homogenization produces a reduction of dispersion due to a loss of K heterogeneity, therefore justifying the inclusion of a term that will represent this loss: the macrodispersion coefficient.

The macrodispersion approach was used to upscale transport at the fine scale, in order to take into account the loss of dispersion caused by hydraulic conductivity upscaling. Block equivalent dispersivities from scenario 2 (see Fig. 3) were used in the transport equation at the coarse scale and BTCs at the control plane were determined. In Fig. 4, it is noticeable that the inclusion of the macrodispersion coefficient in the transport equation at the coarse scale was not enough to properly describe the heterogeneous processes taking place within a block to reproduce the BTC obtained at the fine scale, as also mentioned by others (Fernàndez-Garcia et al., 2009; Fernàndez-Garcia and Gómez-Hernández, 2007; Frippiat and Holeyman, 2008). The slope of the BTC is almost the same, indicating that the dispersion was quantified correctly, however, it seems that the solute arrives earlier in the coarse scale transport model, underestimating the arrival times. A similar result was also mentioned by Fernàndez-Garcia et al. (2009) and can be related to anomalous (non-Fickian) solute transport. To correct the underestimation of the arrival times, the calibration parameter R_f was added. In Fig. 4, it is noticeable that the reproduction at the coarse scale of the fine scale BTC is more precise and presents smaller errors after the inclusion of R_f.

From Fig. 4, we can notice that the efficiency of the macrodispersion method is not the same for the entire BTC, and, according to the solute modeling objective, the ADE approach can be more or less suitable. For this reason, we investigated the results for the early, mean, median and late arrival times to quantify the differences between arrival times at the fine and coarse scales after macrodispersion upscaling. Fig. 5 (a - d) shows, for each of the thirty realizations, the comparison of the mean time and the times when 5%, 50% and 95% of the concentration has arrived at the control plane computed at the fine scale, and at the coarse scale after upscaling using the Macrodispersion approach. It is remarkable that none of the arrival times was well reproduced at the coarse scale by the macrodispersion upscaling, with the worst reproduction obtained for the early times and the best one for the mean arrival times. In all situations analyzed, the Macrodispersion method overestimates the concentrations at any given time. Different results were obtained by Fernàndez-Garcia et al. (2009), Fernàndez-Garcia and Gómez-Hernández (2007) and Cassiraga et al., (2005), where the macrodispersive model was capable of reproducing $T_{05\%}$. In the works by these researchers, the late arrival time ($T_{95\%}$)

of the BTC at the coarse scale was the most poorly reproducing the fine scale values, contrary to our results.

The performance of upscaling after the inclusion of a fictitious retardation factor was also investigated for the early, mean, median and late arrival times. The results are shown in Fig. 6 (a-d). Although the inclusion of a R_f improved the results, it was not enough to reproduce the transport at the coarse scale for the early arrival times. Again, the best results were obtained for the mean arrival times, indicating that this approach can be best suited for performing, for instance, health risk analysis of contamination by drinking water. Results obtained for the median and late arrival times were also good with small relative bias (4.38 % and 3.92 %, respectively).

These results show that without the inclusion of R_f there is no R that can represent the apparently anomalous transport at the coarse scale. As an alternative, upscaling may be done including memory functions to describe the processes leading to slow advection within a block (Fernàndez-Garcia et al., 2009; Li et al., 2011b). However, after the correction using a R_f, a good reproduction of the transport at the coarse scale was obtained for the median, mean and late arrival times. This simple method could promptly be used in daily practice, improving the quality of the solute transport predictions.

5.2. Retardation factor upscaling

Fig. 7 illustrates that different retardation factors must be used to reproduce different parts of the BTC. Since a single R_{eq} is not able to reproduce the entire BTC, retardation factor upscaling was performed considering different R_{eq} for the early, median, mean and late arrival times. The equivalent retardation factor represents not only the chemical heterogeneity, but also the heterogeneity related to hydraulic conductivity, evidenced by the need to include a fictitious retardation factor to properly upscale hydrodynamic dispersion after hydraulic conductivity upscaling. However, as here the aiming was to observe only the effects of chemical heterogeneity, the effect of K heterogeneity on R, represented by R_f, was removed before the calculation of R_b ($R_b = R_{eq} / R_f$).

We investigated the determination of an exponent p for the ensemble of 30 realizations considered altogether. The arithmetic mean (p=1) resulted in the smallest RB_R and,

therefore, was found to be the best approximate for the median, mean and late arrival times. Differently, for the early arrival time the geometric mean (p=0) was the best average. There is no clear indication of systematic under or overestimation of the results, however, using a single p-exponent to predict all the curves gives errors as large as 21%. Because of that, to improve the prediction quality, the block retardation factor was determined using the best p exponent for each realization. Fig. 8 shows the cumulative frequency distribution function of the p exponents from the different realizations found for the early, median, mean and late arrival times. We can observe that they present high variability, ranging from -10.25 to 12.60 with a very similar shape of their CDFs. Fig. 9 presents the comparison of the early, median, mean and late arrival times obtained computed at the fine scale *vs.* the results obtained after upscaling using a different (the best) p-exponent for each realization. All arrival times have a small relative bias and the best result was obtained for the mean arrival time. Our result showed that the upscaling of the retardation factor using a best p-exponent for each realization resulted in a very good coarse-scale reproduction of the reactive transport at the fine scale.

5.3. Uncertainty propagation

Since exhaustive knowledge of the area of interest is unattainable due to the large spatial variability of the parameters and limited sampling, we need to use a stochastic approach for the quantification of uncertainty, where multiple possible scenarios (realizations) are considered. When performing solute transport upscaling, the uncertainty in the upscaled model must be investigated. In this sense, we evaluated how uncertainty propagates after solute transport upscaling.

The cumulative frequency distribution function (CDF) is used to measure the uncertainty about each of the different arrival times. Fig. 10 (a to d) shows the results of the uncertainty reproduction after macrodispersion upscaling by comparing the CDFs of the early (a), median (b), mean (c) and late (d) arrival times at both scales, with and without inclusion of the fictitious retardation factor. We can see that the CDF without R_f is displaced to the left, indicating an overestimation of the concentrations. The inclusion of R_f resulted in a much better reproduction of all arrival times. The uncertainty, related to the slope of the CDF, was well reproduced for all arrival times for the models with and

without the inclusion of the fictitious retardation factor. However, for the early arrival time, even with the inclusion of the fictitious retardation factor there was an overestimation of the concentrations. These results show that the inclusion of R_f in hydrodynamic dispersion upscaling was necessary for the correct reproduction of all arrival times but had no influence on the uncertainty propagation.

We also evaluated the uncertainty propagation after R upscaling. The results are shown in Fig. 11, where the CDF of the early, median, mean and late arrival times obtained at the fine scale are compared with those obtained at the coarse scale using the best exponent p for each realization. We can notice that the larger the arrival time, the larger the uncertainty. The uncertainty was properly propagated for all arrival times. However, the upscaling of R at the late arrival time showed an overestimation of the concentrations.

6. Conclusions

Stochastic solute transport upscaling using real data from a tropical soil was performed. Upscaling of hydraulic conductivity, hydrodynamic dispersion, and retardation factor were done using different techniques of varying complexity. Macrodispersion coefficients were determined considering heterogeneous hydraulic conductivities and dispersivities at the local scale. Upscaling of retardation factor was made by using the p-norm approach. Uncertainty analyses were also performed to evaluate how uncertainty propagates after upscaling.

Upscaling of hydraulic conductivity only, even when using a non-local method, was not enough to reproduce the BTCs at the coarse scale; there is a need to include a macrodispersion coefficient. The Macrodispersion method can be used directly to quantify both the effects of heterogeneity of dispersivity and hydraulic conductivity at the local scale with a small relative bias. However, the inclusion of the macrodispersion coefficient in the transport equation at the coarse scale was not enough to properly describe the heterogeneous processes at the coarse scale. There is a need to include a calibration parameter, a fictitious retardation factor, for the macrodispersion model to get a small relative bias. The retardation factor was well reproduced at the coarse scale when a specific p exponent was used for each realization. The best results were obtained for the

mean arrival times, while the early arrival time resulted in the worst relative bias. The uncertainty was properly propagated after hydrodynamic dispersion upscaling, however, only when a fictitious retardation factor was included there was no overestimation of the contamination. Retardation factor upscaling propagated well the uncertainty for all arrival times. Lastly, the results show that solute transport upscaling can be incorporated into practice by the numerical modeler even using commercial codes, but it may need some corrections with the need to include a fictitious retardation factor in some cases.

Acknowledgments

The authors thank the financial support by the Brazilian National Council for Scientific and Technological Development (CNPq) (Project 401441/2014-8). The doctoral fellowship award to the first author by the Coordination of Improvement of Higher Level Personnel (CAPES) is acknowledged. The first author also thanks the international mobility grant awarded by CNPq, through the Sciences Without Borders program (grant number: 200597/2015-9). The international mobility grant awarded by Santander Mobility in cooperation with the University of Sao Paulo is also acknowledged. DHI-WASI is gratefully thanked for providing a FEFLOW license.

References

Ahuja, L.R., Naney, J.W., Green, R.E., Nielsen, D.R., 1984. Macroporosity to Characterize Spatial Variability of Hydraulic Conductivity and Effects of Land Management1. Soil Sci. Soc. Am. J. 48:, 699. https://doi.org/10.2136/sssaj1984.03615995004800040001x

Azevedo, A.A.B. de, Pressinotti, M.M.N., Massoli, M., 1981. Sedimentological studies of the Botucatu and Pirambóia formations in the region of Santa Rita do Passa Quatro (In portuguese). Rev. do Inst. Geológico 2:, 31–38. https://doi.org/10.5935/0100-929X.19810003

Bellin, A., Lawrence, A.E., Rubin, Y., 2004. Models of sub-grid variability in numerical simulations of solute transport in heterogeneous porous formations: three-dimensional flow and effect of pore-scale dispersion. Stoch. Environ. Res. Risk Assess. 18:, 31–38. https://doi.org/10.1007/s00477-003-0164-2

Brent, R.P., 1973. Algorithms for Minimization without Derivatives. Prentice Hall, Englewood cliffs, New Jersey.

Brusseau, M.L., 1998. Non-ideal transport of reactive solutes in heterogeneous porous media: 3. model testing and data analysis using calibration versus prediction. J. Hydrol. 209:, 147–165. https://doi.org/10.1016/S0022-1694(98)00121-8

Brusseau, M.L., Srivastava, R., 1999. Nonideal transport of reactive solutes in heterogeneous porous media: 4. Analysis of the Cape Cod Natural-Gradient Field Experiment. Water Resour. Res. 35:, 1113–1125. https://doi.org/10.1029/1998WR900019

Brutsaert, W., 1967. Some methods of calculating unsaturated permeability. Trans. ASAE 10:, 400–404.

Cadini, F., De Sanctis, J., Bertoli, I., Zio, E., 2013. Upscaling of a dual-permeability Monte Carlo simulation model for contaminant transport in fractured networks by genetic algorithm parameter identification. Stoch. Environ. Res. Risk Assess. 27:, 505–516. https://doi.org/10.1007/s00477-012-0595-8

Cambardella, C.A., Moorman, T.B., Parkin, T.B., Karlen, D.L., Novak, J.M., Turco, R.F., Konopka, A.E., 1994. Field-Scale Variability of Soil Properties in Central Iowa Soils. Soil Sci. Soc. Am. J. 58:, 1501. https://doi.org/10.2136/sssaj1994.03615995005800050033x

Capilla, J.E., Rodrigo, J., Gómez-Hernández, J.J., 1999. Simulation of non-Gaussian transmissivity fields honoring piezometric data and integrating soft and secondary information. Math. Geol. 31:, 907–927. https://doi.org/10.1023/A:1007580902175

Cassiraga, E.F., Fernàndez-Garcia, D., Gómez-Hernández, J.J., 2005. Performance assessment of solute transport upscaling methods in the context of nuclear waste disposal. Int. J. Rock Mech. Min. Sci. 42:, 756–764. https://doi.org/10.1016/j.ijrmms.2005.03.013

Corey, A.T., 1977. Mechanics of heterogeneous fluids in porous media. Mech. Heterog. fluids porous media.

Dagan, G., 2004. On application of stochastic modeling of groundwater flow and transport. Stoch. Environ. Res. Risk Assess. 18:. https://doi.org/10.1007/s00477-004-0191-7

Dagan, G., 1989. Flow and Transport in Porous Formations. Springer Berlin Heidelberg, Berlin, Heidelberg. https://doi.org/10.1007/978-3-642-75015-1

Deng, H., Dai, Z., Wolfsberg, A. V., Ye, M., Stauffer, P.H., Lu, Z., Kwicklis, E., 2013. Upscaling retardation factor in hierarchical porous media with multimodal reactive mineral facies. Chemosphere 91:, 248–257. https://doi.org/10.1016/j.chemosphere.2012.10.105

Diersch, H.-J.G., 2014. Finite Element Modeling of Flow, Mass and Heat Transport in Porous and Fractured Media. https://doi.org/10.1007/978-3-642-38739-5

Dippenaar, M.A., 2014. Porosity Reviewed: Quantitative Multi-Disciplinary Understanding, Recent Advances and Applications in Vadose Zone Hydrology. Geotech. Geol. Eng. 32:, 1–19. https://doi.org/10.1007/s10706-013-9704-9

Fagundes, J.R.T., Zuquette, L.V., 2011. Sorption behavior of the sandy residual

unconsolidated materials from the sandstones of the Botucatu Formation, the main aquifer of Brazil. Environ. Earth Sci. 62:, 831–845. https://doi.org/10.1007/s12665-010-0570-y

Fernàndez-Garcia, D., Gómez-Hernández, J.J., 2007. Impact of upscaling on solute transport: Traveltimes, scale dependence of dispersivity, and propagation of uncertainty. Water Resour. Res. 43:. https://doi.org/10.1029/2005WR004727

Fernàndez-Garcia, D., Llerar-Meza, G., Gómez-Hernández, J.J., 2009. Upscaling transport with mass transfer models: Mean behavior and propagation of uncertainty. Water Resour. Res. 45:. https://doi.org/10.1029/2009WR007764

Feyen, L., Gómez-Hernández, J.J., Ribeiro, P.J., Beven, K.J., De Smedt, F., 2003a. A Bayesian approach to stochastic capture zone delineation incorporating tracer arrival times, conductivity measurements, and hydraulic head observations. Water Resour. Res. 39:. https://doi.org/10.1029/2002WR001544

Feyen, L., Ribeiro, P.J., Gómez-Hernández, J.J., Beven, K.J., De Smedt, F., 2003b. Bayesian methodology for stochastic capture zone delineation incorporating transmissivity measurements and hydraulic head observations. J. Hydrol. 271:, 156–170. https://doi.org/10.1016/S0022-1694(02)00314-1

Forsythe, G.E., Malcolm, M.A., Moler, C.B., 1976. Computer Methods for Mathematical Computations. Englewood Cliffs. Prentice-Hall, Englewood cliffs, New Jersey. https://doi.org/0131653326

Freeze, R., Cherry, J., 1979. Groundwater (p. 604). PrenticeHall Inc Englewood cliffs, New Jersey.

Frippiat, C.C., Holeyman, A.E., 2008. A comparative review of upscaling methods for solute transport in heterogeneous porous media. J. Hydrol. 362:, 150–176. https://doi.org/10.1016/j.jhydrol.2008.08.015

Fu, J., Gómez-Hernández, J.J., 2009. Uncertainty assessment and data worth in groundwater flow and mass transport modeling using a blocking Markov chain Monte Carlo method. J. Hydrol. 364:, 328–341.

https://doi.org/10.1016/j.jhydrol.2008.11.014

Gelhar, L.W., Axness, C.L., 1983. Three-dimensional stochastic analysis of macrodispersion in aquifers. Water Resour. Res. 19:, 161–180. https://doi.org/10.1029/WR019i001p00161

Gelhar, L.W., Welty, C., Rehfeldt, K.R., 1992. A critical review of data on field-scale dispersion in aquifers. Water Resour. Res. 28:, 1955–1974. https://doi.org/10.1029/92WR00607

Giacheti, H.L., Rohm, S.A., Nogueira, J.B., Cintra, J.C.A., 1993. Geotechnical properties of the Cenozoic sediment (In protuguese), in: Albiero, J.H., Cintra, J.C.A. (Eds.), Soil from the Interior of São Paulo. ABMS, Sao Paulo, pp. 143–175.

Gómez-Hernandez, J.J., 1990. A stochastic approach to the simulation of block conductivity fields conditional upon data measured at a smaller scale. Stanford University.

Gómez-Hernández, J.J., Fu, J., Fernandez-Garcia, D., 2006. Upscaling retardation factors in 2-D porous media, in: Bierkens, M.F.P., Gehrels, J.C., Kovar, K. (Eds.), Calibration and Reliability in Groundwater Modelling : From Uncertainty to Decision Making : Proceedings of the ModelCARE 2005 Conference Held in The Hague, the Netherlands, 6-9 June, 2005. IAHS Publication, pp. 130–136.

Gómez-Hernández, J.J., Gorelick, S.M., 1989. Effective groundwater model parameter values: Influence of spatial variabiity of hydraulic conductivity, leackance, and recharge. Water Resour. Res. 25:, 405–419.

Gómez-Hernández, J.J., Journel, A., 1993. Joint Sequential Simulation of MultiGaussian Fields, in: Geostatistics Tróia ’92. pp. 85–94. https://doi.org/10.1007/978-94-011-1739-5_8

Gómez-Hernández, J.J., Wen, X.-H., 1994. Probabilistic assessment of travel times in groundwater modeling. Stoch. Hydrol. Hydraul. 8:, 19–55. https://doi.org/10.1007/BF01581389

Goovaerts, P., 1999. Geostatistics in soil science: State-of-the-art and perspectives.

Geoderma 89:, 1–45. https://doi.org/10.1016/S0016-7061(98)00078-0

Griffiths, D. V., Fenton, G. a., 2008. Risk Assessment in Geotechnical Engineering.

Jarvis, N.J., 2007. A review of non-equilibrium water fl ow and solute transport in soil macropores: Principles, controlling factors and consequences for water quality. Eur. J. Soil Sci. 58:, 523–546. https://doi.org/10.4141/cjss2011-050

Jellali, S., Diamantopoulos, E., Kallali, H., Bennaceur, S., Anane, M., Jedidi, N., 2010. Dynamic sorption of ammonium by sandy soil in fixed bed columns: Evaluation of equilibrium and non-equilibrium transport processes. J. Environ. Manage. 91:, 897–905. https://doi.org/10.1016/j.jenvman.2009.11.006

Journel, A., Deutsch, C., Desbarats, A., 1986. Power averaging for block effective permeability. Proc. SPE Calif. Reg. Meet. https://doi.org/10.2118/15128-MS

Journel, A.G., Gomez-Hernandez, J.J., 1993. Stochastic Imaging of the Wilmington Clastic Sequence. SPE Form. Eval. 8:, 33–40. https://doi.org/10.2118/19857-PA

Kronberg, B.I., Fyfe, W.S., Leonardos, O.H., Santos, A.M., 1979. The chemistry of some Brazilian soils: Element mobility during intense weathering. Chem. Geol. 24:, 211–229. https://doi.org/10.1016/0009-2541(79)90124-4

Lake, L.W., 1988. The Origins of Anisotropy (includes associated papers 18394 and 18458). J. Pet. Technol. 40:, 395–396. https://doi.org/10.2118/17652-PA

Lawrence, A.E., Rubin, Y., 2007. Block-effective macrodispersion for numerical simulations of sorbing solute transport in heterogeneous porous formations. Adv. Water Resour. 30:, 1272–1285. https://doi.org/10.1016/j.advwatres.2006.11.005

Lemke, L.D., Barrack II, W.A., Abriola, L.M., Goovaerts, P., 2004. Matching Solute Breakthrough with Deterministic and Stochastic Aquifer Models. Groundwater 42:, 920–934.

Li, L., Zhou, H., Gómez-Hernández, J.J., 2011a. A comparative study of three-dimensional hydraulic conductivity upscaling at the macro-dispersion experiment (MADE) site, Columbus Air Force Base, Mississippi (USA). J. Hydrol. 404:, 278–

293. https://doi.org/10.1016/j.jhydrol.2011.05.001

Li, L., Zhou, H., Gómez-Hernández, J.J., 2011b. Transport upscaling using multi-rate mass transfer in three-dimensional highly heterogeneous porous media. Adv. Water Resour. 34:, 478–489. https://doi.org/10.1016/j.advwatres.2011.01.001

Logsdon Keller, K.E., Moorman, T.B., 2002. Measured and Predicted Solute Leaching from Multiple Undisturbed Soil Columns. Soil Sci. Soc. am. J. 66:, 686–695. https://doi.org/10.2136/sssaj2002.6860

Lourens, A., van Geer, F.C., 2016. Uncertainty propagation of arbitrary probability density functions applied to upscaling of transmissivities. Stoch. Environ. Res. Risk Assess. 30:, 237–249. https://doi.org/10.1007/s00477-015-1075-8

Mahapatra, I.C., Singh, K.N., Pillai, K.G., Bapat, S.R., 1985. Rice soils and their management. Indian J. Agron. 1–41.

Morakinyo, J.A., Mackay, R., 2006. Geostatistical modelling of ground conditions to support the assessment of site contamination. Stoch. Environ. Res. Risk Assess. 20:, 106–118. https://doi.org/10.1007/s00477-005-0015-4

Moslehi, M., de Barros, F.P.J., Ebrahimi, F., Sahimi, M., 2016. Upscaling of solute transport in disordered porous media by wavelet transformations. Adv. Water Resour. 96:, 180–189. https://doi.org/10.1016/j.advwatres.2016.07.013

Osinubi, K. ‘J., Nwaiwu, C.M., 2005. Hydraulic Conductivity of Compacted Lateritic Soil. J. Geotech. Geoenvironmental Eng. 131:, 1034–1041. https://doi.org/10.1061/(ASCE)1090-0241(2005)131:8(1034)

Remy, N., 2004. SGeMS: Stanford Geostatistical Modeling Software. Softw. Man. https://doi.org/10.1007/978-1-4020-3610-1_89

Renard, P., de Marsily, G., 1997. Calculating equivalent permeability: a review. Adv. Water Resour. 20:, 253–278. https://doi.org/10.1016/S0309-1708(96)00050-4

Robin, M.J.L., Sudicky, E.A., Gillham, R.W., Kachanoski, R.G., 1991. Spatial Variability of Strontium Distribution Coefficients and Their Correlation With Hydraulic

Conductivity in the Canadian Forces Base Borden Aquifer. Water Resour. Res. 27:, 2619–2632. https://doi.org/10.1029/91WR01107

Salamon, P., Fernàndez-Garcia, D., Gómez-Hernández, J.J., 2007. Modeling tracer transport at the MADE site: The importance of heterogeneity. Water Resour. Res. 43:. https://doi.org/10.1029/2006WR005522

Sánchez-Vila, X., Carrera, J., Girardi, J.P., 1996. Scale effects in transmissivity. J. Hydrol. 183:, 1–22. https://doi.org/10.1016/S0022-1694(96)80031-X

Scheibe, T., Yabusaki, S., 1998. Scaling of flow and transport behavior in heterogeneous groundwater systems. Adv. Water Resour. 22:, 223–238. https://doi.org/10.1016/S0309-1708(98)00014-1

Selvadurai, P.A., Selvadurai, A.P.S., 2014. On the effective permeability of a heterogeneous porous medium: the role of the geometric mean. Philos. Mag. 94:, 2318–2338. https://doi.org/10.1080/14786435.2014.913111

Shackelford, C.D., 1994. Critical concepts for column testing. J. Geotech. Eng. 120:, 1804–1828. https://doi.org/10.1016/0148-9062(95)96996-O

Šimůnek, J., van Genuchten, M.T., Šejna, M., Toride, N., Leij, F.J., 1999. The STANMOD Computer Software for Evaluating Solute Transport in Porous Media Using Analytical Solutions of Convection-Dispersion Equation. Riverside, California.

Taskinen, A., Sirviö, H., Bruen, M., 2008. Modelling effects of spatial variability of saturated hydraulic conductivity on autocorrelated overland flow data: linear mixed model approach. Stoch. Environ. Res. Risk Assess. 22:, 67–82. https://doi.org/10.1007/s00477-006-0099-5

Tuli, A., Hopmans, J.W., Rolston, D.E., Moldrup, P., 2005. Comparison of Air and Water Permeability between Disturbed and Undisturbed Soils. Soil Sci. Soc. Am. J. 69:, 1361. https://doi.org/10.2136/sssaj2004.0332

Tyukhova, A.R., Willmann, M., 2016. Conservative transport upscaling based on information of connectivity. Water Resour. Res. 52:, 6867–6880. https://doi.org/10.1002/2015WR018331

van Genuchten, M.T., 1980. Determining transport parameters from solute displacement experiments.

Vanderborght, J., Timmerman, A., Feyen, J., 2000. Solute Transport for Steady-State and Transient Flow in Soils with and without Macropores. Soil Sci. Soc. Am. J. 64:, 1305–1317. https://doi.org/10.2136/sssaj2000.6441305x

Vanmarcke, E., 1983. Random Fields: Analysis and Synthesis.

Vishal, V., Leung, J.Y., 2017. Statistical scale-up of 3D particle-tracking simulation for non-Fickian dispersive solute transport modeling. Stoch. Environ. Res. Risk Assess. https://doi.org/10.1007/s00477-017-1501-1

Wen, X.-H., Gómez-Hernández, J.J., 1996. Upscaling hydraulic conductivities in heterogeneous media: An overview. J. Hydrol. 183:, ix–xxxii. https://doi.org/10.1016/S0022-1694(96)80030-8

Wen, X.H., Capilla, J.E., Deutsch, C.V., Gómez-Hernández, J.J., Cullick, A.S., 1999. A program to create permeability fields that honor single-phase flow rate and pressure data. Comput. Geosci. 25:, 217–230. https://doi.org/10.1016/S0098-3004(98)00126-5

Wen, X.H., Gómez-Hernández, J.J., 1998. Numerical modeling of macrodispersion in heterogeneous media: a comparison of multi-Gaussian and non-multi-Gaussian models. J. Contam. Hydrol. 30:, 129–156. https://doi.org/10.1016/S0169-7722(97)00035-1

Wilding, L.P., Drees, L.R., 1983. Spatial variability and pedology, in: Wilding, L.P., Smeck, N.E., Hall, G.F. (Eds.), Pedogenesis and Soil Taxonomy : The Soil Orders. Elsevier, Netherlands, pp. 83–116.

Willmann, M., Carrera, J., Guadagnini, A., 2006. Block-upscaling of transport in heterogeneous aquifers. h2ogeo.upc.edu 1–7.

Xu, Z., Meakin, P., 2013. Upscaling of solute transport in heterogeneous media with non-uniform flow and dispersion fields. Appl. Math. Model. 37:, 8533–8542. https://doi.org/10.1016/j.apm.2013.03.070

Zech, A., Attinger, S., Cvetkovic, V., Dagan, G., Dietrich, P., Fiori, A., Rubin, Y., Teutsch, G., 2015. Is unique scaling of aquifer macrodispersivity supported by field data? Water Resour. Res. 51:, 7662–7679. https://doi.org/10.1002/2015WR017220

Zhou, H., Li, L., Gómez-Hernández, J.J., 2010. Three-dimensional hydraulic conductivity upscaling in groundwater modeling. Comput. Geosci. 36:, 1224–1235. https://doi.org/10.1016/j.cageo.2010.03.008

Zhou, H., Li, L., Hendricks Franssen, H.-J., Gómez-Hernández, J.J., 2012. Pattern Recognition in a Bimodal Aquifer Using the Normal-Score Ensemble Kalman Filter. Math. Geosci. 44:, 169–185. https://doi.org/10.1007/s11004-011-9372-3

List of Figures

Fig. 9 Comparison of the early (a), median (b), mean (c) and late (d) arrival times obtained from the model performed at fine-scale versus the results obtained after upscaling using the best p exponent for the entire ensemble

Fig. 10 Cumulative frequency distribution functions of the early (a), median (b), mean (c) and late (d) arrival times obtained from the nonreactive BTCs computed at the fine scale versus the results obtained after upscaling using only macrodispersion coefficients and using macrodispersion coefficients plus a fictitious retardation factor

Fig. 11 Cumulative frequency distribution of the early, median, mean and late arrival times obtained from the reactive BTCs before and after upscaling using the best p exponent for each realization

Fig. 1

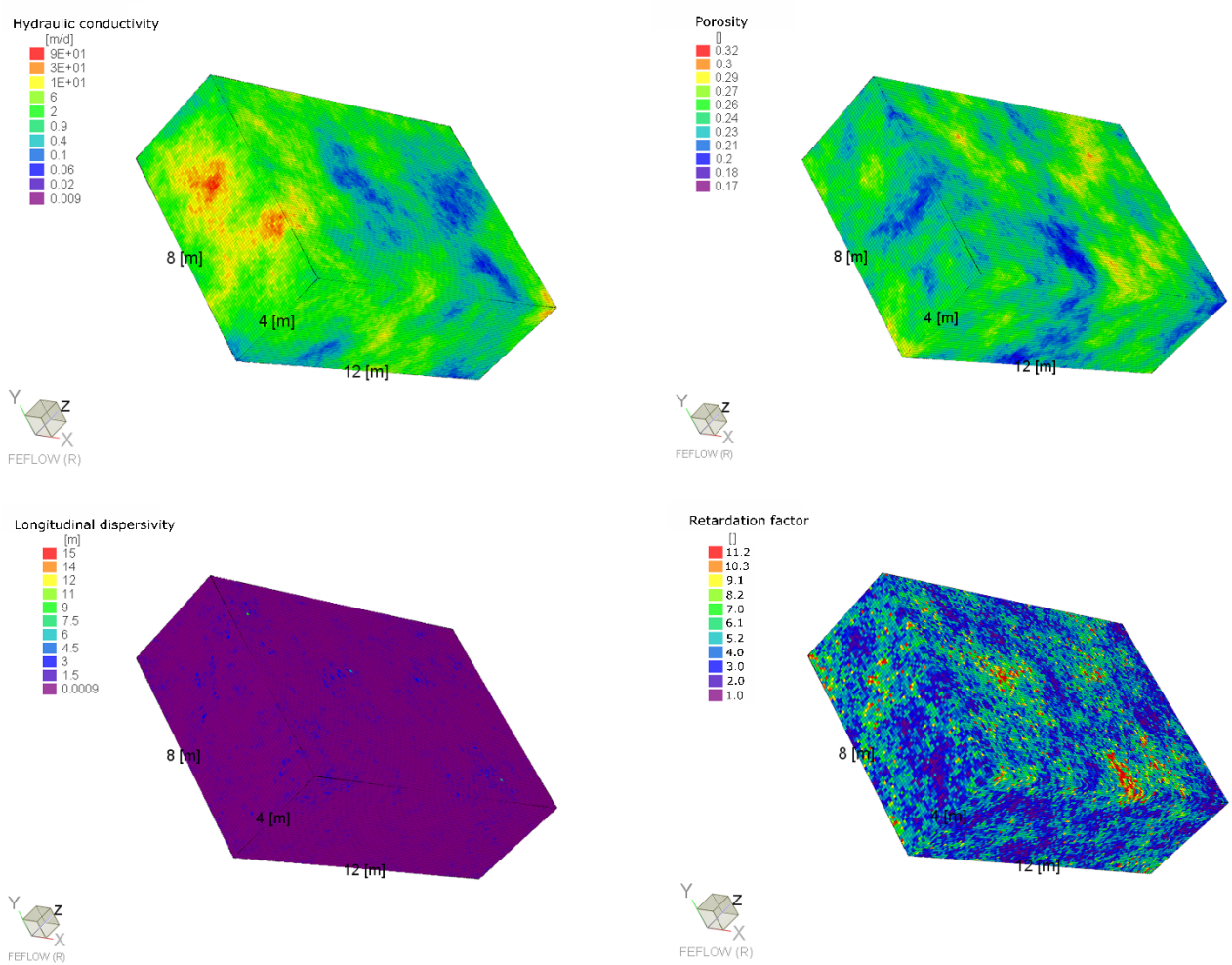
Hydraulic conductivity
[m/d]
9E+01
3E+01
1E+01
6
2
0.9
0.4
0.1
0.06
0.02
0.009
8 [m]
4 [m]
12 [m]
Y
Z
X
FEFLOW (R)
Porosity
[]
0.32
0.3
0.29
0.27
0.26
0.24
0.23
0.21
0.2
0.18
0.17
8 [m]
4 [m]
12 [m]
Y
Z
X
FEFLOW (R)
Longitudinal dispersivity
[m]
15
14
12
11
9
7.5
6
4.5
3
1.5
0.0009
8 [m]
4 [m]
12 [m]
Y
Z
X
FEFLOW (R)
Retardation factor
[]
11.2
10.3
9.1
8.2
7.0
6.1
5.2
4.0
3.0
2.0
1.0
8 [m]
4 [m]
12 [m]
Y
Z
X
FEFLOW (R)

Fig. 2

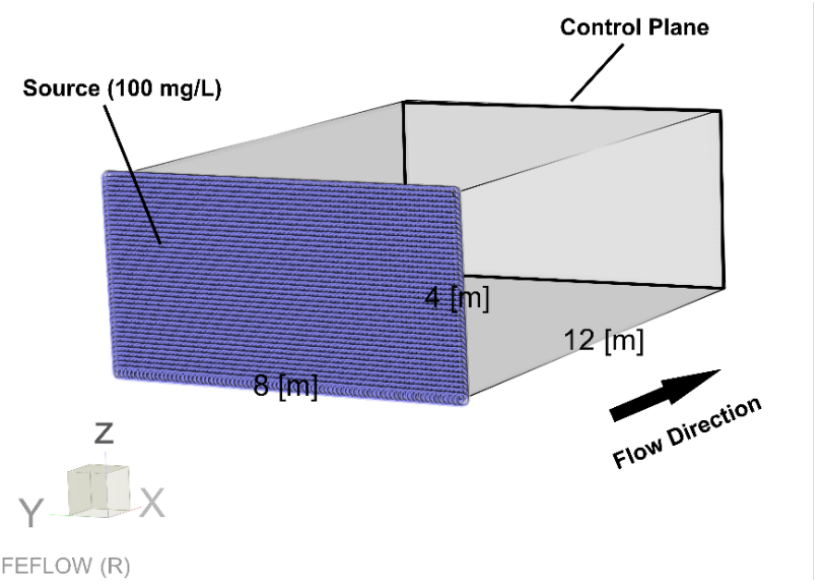
Control Plane
Source (100 mg/L)
4 [m]
12 [m]
8 [m]
Flow Direction
Z
Y
X
FEFLOW (R)

Fig. 3

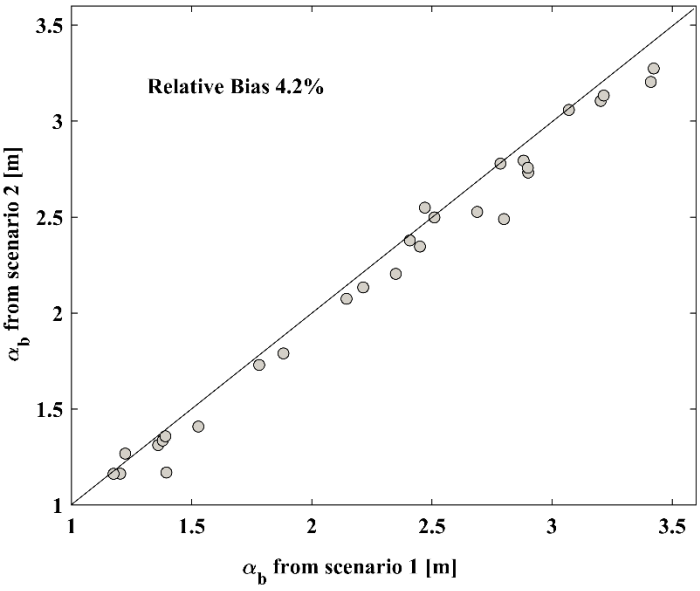
Relative Bias 4.2%
α_b from scenario 2 [m]
α_b from scenario 1 [m]
3.5
3
2.5
2
1.5
1
1
1.5
2
2.5
3
3.5

Fig. 4

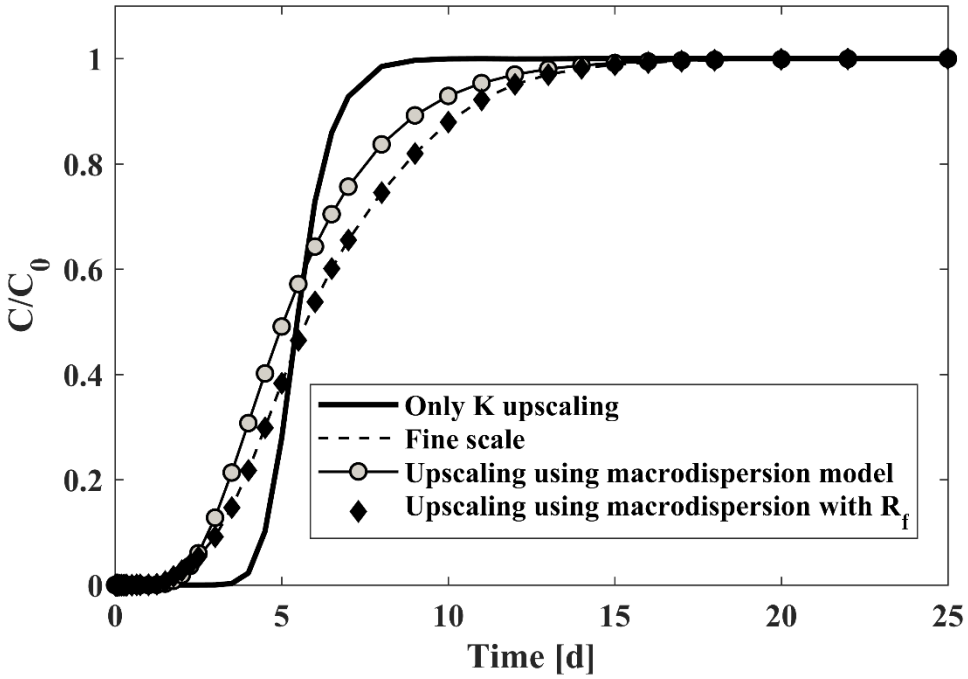
C/C0
Time [d]
Only K upscaling
Fine scale
Upscaling using macrodispersion model
Upscaling using macrodispersion with Rf

Fig. 5

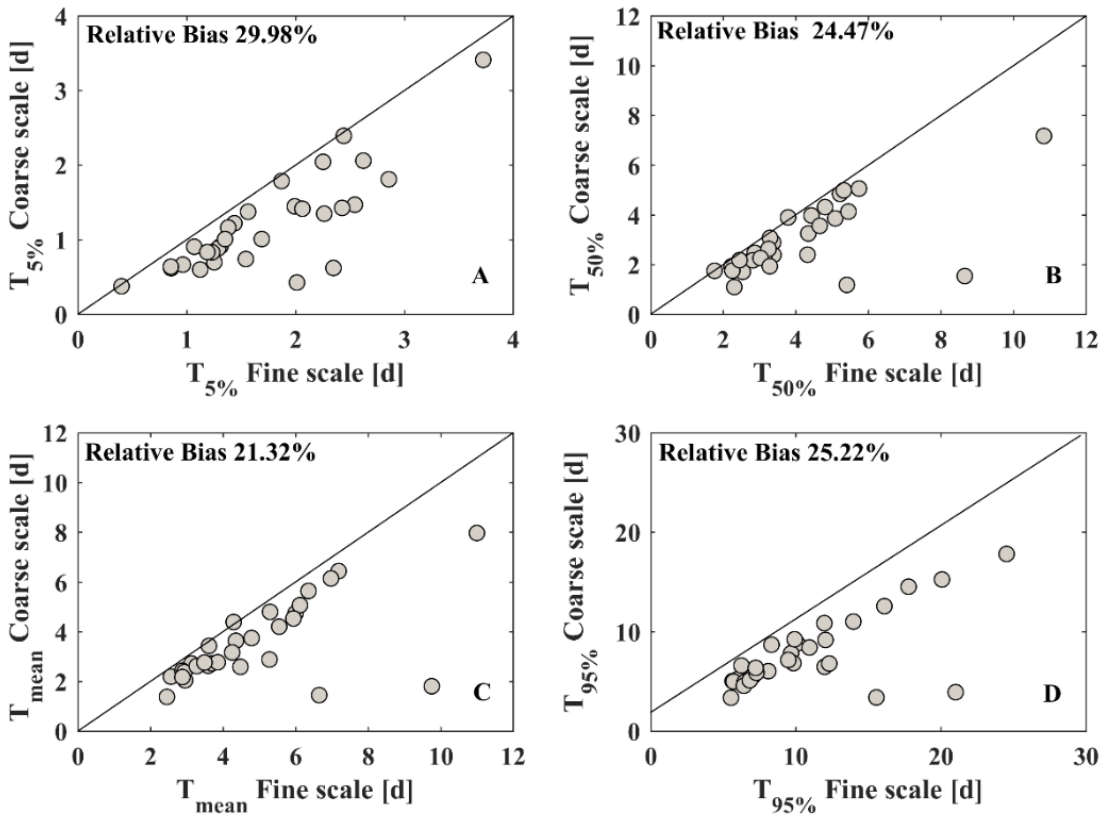
Relative Bias 29.98%
$T_{5\%}$ Coarse scale [d]
$T_{5\%}$ Fine scale [d]
A
Relative Bias 24.47%
$T_{50\%}$ Coarse scale [d]
$T_{50\%}$ Fine scale [d]
B
Relative Bias 21.32%
T_{mean} Coarse scale [d]
T_{mean} Fine scale [d]
C
Relative Bias 25.22%
$T_{95\%}$ Coarse scale [d]
$T_{95\%}$ Fine scale [d]
D

Fig. 6

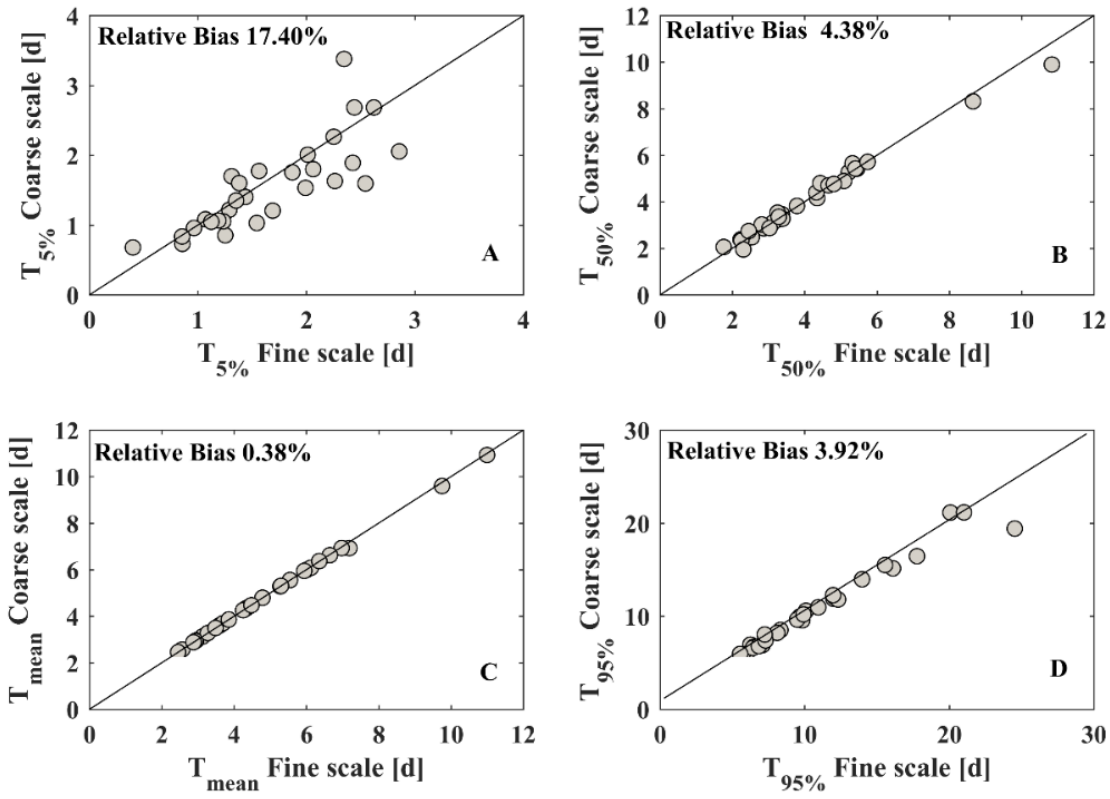
Relative Bias 17.40%
A
$T_{5\%}$ Coarse scale [d]
$T_{5\%}$ Fine scale [d]
Relative Bias 4.38%
B
$T_{50\%}$ Coarse scale [d]
$T_{50\%}$ Fine scale [d]
Relative Bias 0.38%
C
T_{mean} Coarse scale [d]
T_{mean} Fine scale [d]
Relative Bias 3.92%
D
$T_{95\%}$ Coarse scale [d]
$T_{95\%}$ Fine scale [d]

Fig. 7

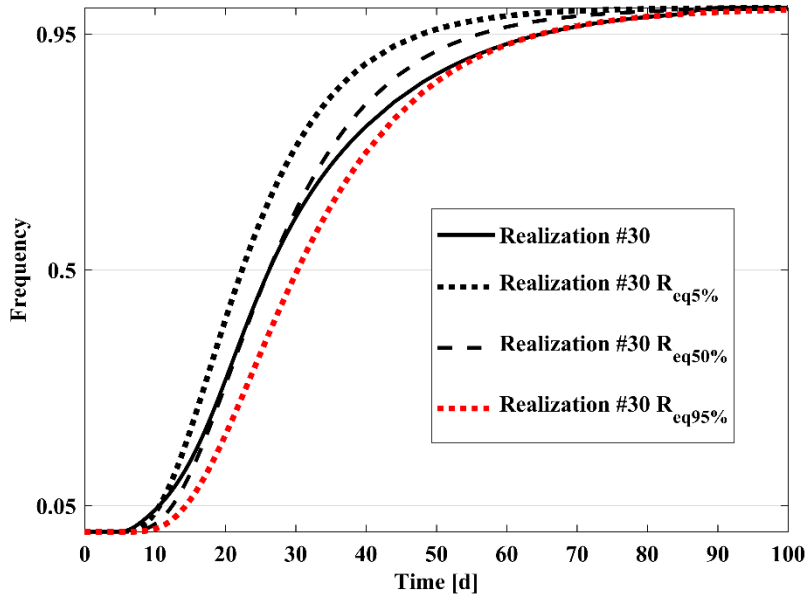
0.95
0.5
0.05
Frequency
0
10
20
30
40
50
60
70
80
90
100
Time [d]
Realization #30
Realization #30 R eq5%
Realization #30 R eq50%
Realization #30 R eq95%

Fig. 8

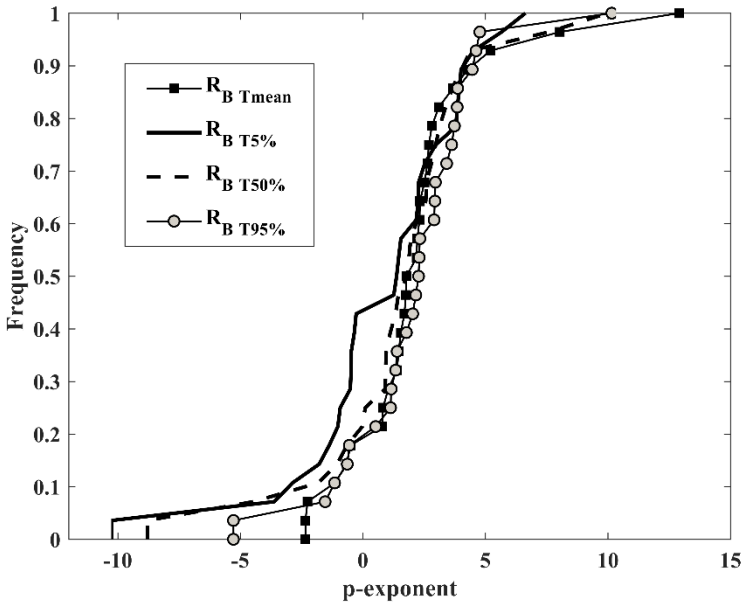
R B Tmean
R B T5%
R B T50%
R B T95%
Frequency
p-exponent
1
0.9
0.8
0.7
0.6
0.5
0.4
0.3
0.2
0.1
0
-10
-5
0
5
10
15

Fig. 9

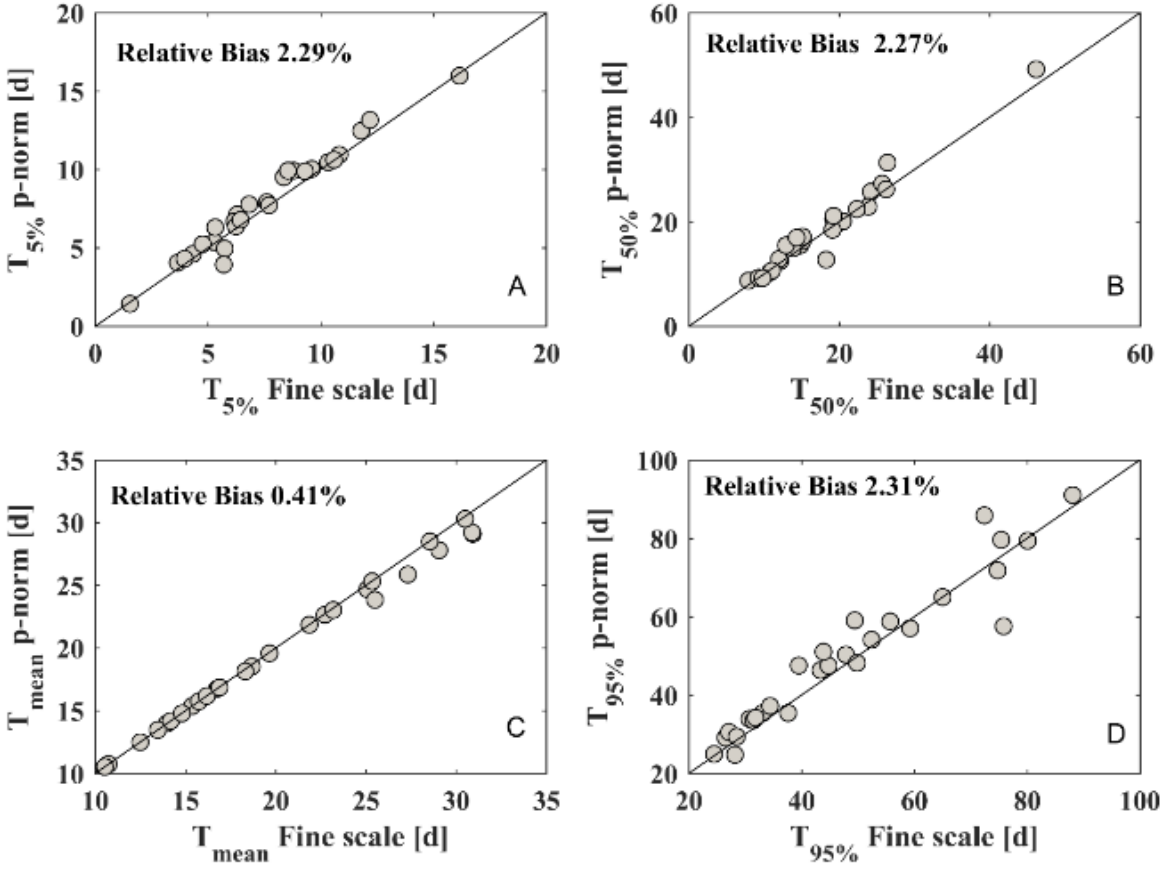
Relative Bias 2.29%
A
$T_{5\%}$ p-norm [d]
$T_{5\%}$ Fine scale [d]
Relative Bias 2.27%
B
$T_{50\%}$ p-norm [d]
$T_{50\%}$ Fine scale [d]
Relative Bias 0.41%
C
T_{mean} p-norm [d]
T_{mean} Fine scale [d]
Relative Bias 2.31%
D
$T_{95\%}$ p-norm [d]
$T_{95\%}$ Fine scale [d]

Fig. 10

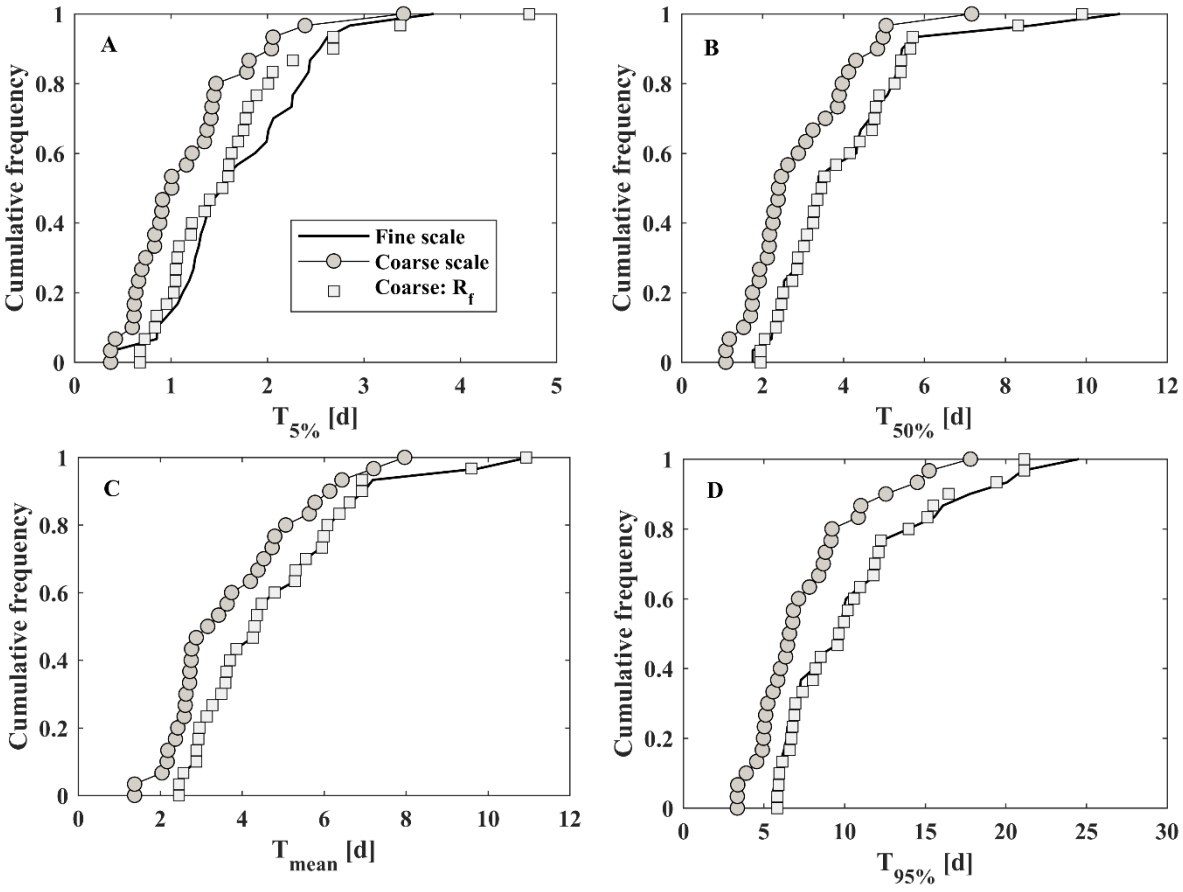
A
B
C
D
Cumulative frequency
Fine scale
Coarse scale
Coarse: R_f
$T_{5\%}$ [d]
$T_{50\%}$ [d]
T_{mean} [d]
$T_{95\%}$ [d]

Fig. 11

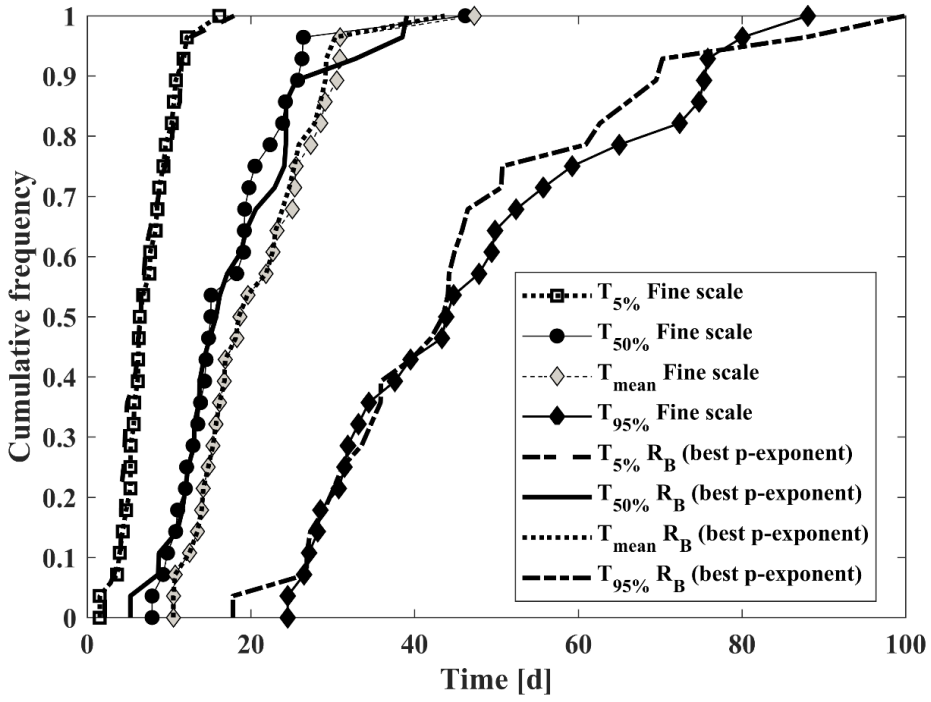
Cumulative frequency
Time [d]
0
0.1
0.2
0.3
0.4
0.5
0.6
0.7
0.8
0.9
1
0
20
40
60
80
100
T5% Fine scale
T50% Fine scale
Tmean Fine scale
T95% Fine scale
T5% RB (best p-exponent)
T50% RB (best p-exponent)
Tmean RB (best p-exponent)
T95% RB (best p-exponent)

List of Tables

1 Table 1

Variable	Mean	SD	CV
K [m d^{-1}]	1.35	1.65	1.26
lnK [ln(m d^{-1})]	-0.38	1.25	n.d
n [ ]	0.25	0.02	0.08
α [m]	0.18	0.19	1.05
lnα [ln(m)]	-2.21	1.11	n.d
R [ ]	5.37	5.10	0.95

2 SD: standard deviation, CV: coefficient of variation, n.d: undetermined, K: hydraulic conductivity;

3 n: porosity, R: retardation factor, α: dispersivity

1 Table 2

Variable	Model	Nugget	Sill	Range (m)
lnK	Spherical	0.00	1.0	4.0
n	Spherical	0.00	1.0	3.0
lnα	Spherical	0.50	0.50	3.0
R	Spherical	0.55	0.45	3.3

2 K: hydraulic conductivity; n: porosity, R: retardation factor, α: dispersivity

3

Table 3

Scenario	K (at fine scale)	α (at fine scale)	Initial Result	Result
Scenario 1	Homogeneous	Heterogeneous	α_{eq}	α_b
	Heterogeneous	Homogeneous	A_i	
Scenario 2	Heterogeneous	Heterogeneous	α_b	α_b

α_{eq}: equivalent fine-scale local dispersivity; A_i: macrodispersivity term; α_b: block equivalent dispersivity.